

## **Preparation of Ti/PbO<sub>2</sub>-ZrO<sub>2</sub> Composite Anode for Zn Electrowinnig**

*Wenrong Cui, Zhen Chen\*, Qiang Yu, Wei Zhu, Huixi Li, and Hong Wang*

Faculty of Science, Kunming University of Science and Technology, Kunming 650093, People's Republic of China

\*E-mail: [chenzhen69@qq.com](mailto:chenzhen69@qq.com)

*Received: 16 August 2017 / Accepted: 20 November 2017 / Published: 28 December 2017*

To improve the oxygen evolution electrocatalytic activity of Ti/β-PbO<sub>2</sub> in zinc electrowinning, the Ti/β-PbO<sub>2</sub>-ZrO<sub>2</sub> electrodes were prepared by anodic oxidation electrodeposition in the lead nitrate plating bath containing ZrO<sub>2</sub> nanoparticles. It was found that the addition of ZrO<sub>2</sub> nanoparticles can obviously increase the effective area of the electrode surface, thus increasing the number of electrode material surface active sites, and has significantly improved the effect of the electrode materials on the electric catalytic activity. SEM and XRD were used to characterize the microstructure and phase composition of the active layer. The electrochemical methods elucidate the role of anode electrolytic zinc composite materials in the oxygen evolution electric catalytic activity. Through the measurement and analysis of cyclic voltammetric curves, we thoroughly discuss the anode composite materials used for electrical deposition of zinc anode and the addition of ZrO<sub>2</sub> activity of nanoparticles on the electrode surface active sites. The results show that for the titanium base after doping ZrO<sub>2</sub> nanoparticles with lead dioxide in the electrolytic zinc liquid, the oxygen evolution potential decreased by approximately 0.28 V, and the electrode surface active surface area increased, with the electrochemical active surface charge number and double electric catalytic activity increasing significantly. The anodic polarization curves show that when doping ZrO<sub>2</sub> nanoparticles into the Ti/β-PbO<sub>2</sub>-ZrO<sub>2</sub> electrodes, the oxygen evolution potential decreased by approximately 0.28 V, and the cyclic voltammetric curves show that the relative surface area of the Ti/β-PbO<sub>2</sub>-ZrO<sub>2</sub> composite electrodes is approximately two times larger than that of the Ti/β-PbO<sub>2</sub> electrodes.

**Keywords:** lead dioxide; ZrO<sub>2</sub> nanoparticles; active sites; oxygen evolution electrocatalytic activity

### **1. INTRODUCTION**

The anode material plays an important role in stabilizing the electrolyte and improving the quality of the cathode in the modern electrolysis industry[1]. Currently, the most widely used materials in zinc electrowinning anodes are the lead based alloy anode and the titanium based coating anode

(DSA anode). While lead based alloy anodes have been used for many years, these materials have many critical drawbacks, such as high cost, high energy consumption, low current efficiency, low mechanical strength, poor corrosion resistance and electrical conductivity, short service life as well as the high impurity content of lead[2-6]. Recently, the titanium-based coating anode has been widely used because of its stable size, long service life, lack of dissolution, high current density, strong corrosion resistance and low weight[7,8]. This anode has been widely studied and applied in many fields, such as metallurgy, electroplating, sewage treatment, ozone generation and so on[1,9-11]. In the extraction of nonferrous metals, this kind of anode can improve the quality of cathode products, reduce the overpotential of oxygen evolution, and shows strong corrosion resistance and other advantages. Therefore, in the electrolysis industry, this anode has attracted wide attention.

Similarly, lead dioxide has the advantageous properties of good electrical conductivity, easy manufacturing, low cost, low resistivity, and high current efficiency and when used as the anode, also shows good catalytic activity, good corrosion resistance[6,12]. Due to its high current characteristics and insoluble anode, lead dioxide is widely used in electrochemical industries; in recent years, lead dioxide has been gradually applied to the electrolysis industry, attracting intense research and development attention as the energy saving type anode material in the extraction of the non-ferrous metals [13-15]. It has been shown that the pure dioxide electrode is used to zinc electrowinning only to show the secondary activity[16]. However, the use of  $F^-$ ,  $Co^{2+}$ ,  $Fe^{3+}$ , and rare earth ions obviously improved the performance[17-19]. Therefore, the main task of current research is to reduce the oxygen potential and improve the catalytic activity of this material. It is well-known that electrochemical properties of electrode materials depend not only on their chemical composition but also on their microstructure, grain size and other physical properties[20,21]. To further improve the electrocatalytic activity of electrode materials, some researchers have introduced a middle layer between the substrate and the active layer[22]. Some researchers also doped functional particles such as metal oxides  $Co_3O_4$ ,  $RuO_2$  and  $TiO_2$  into the parent lead dioxide[16,23-25]. The electrodes are modified to improve electrochemical properties. Previous research indicates that the doping of metal oxide has a significant effect on the performance of electrode materials[26]. In this work, the electrocatalytic properties of the composite electrode are shown to be especially affected by their composition and microstructure.

$Ti/\beta-PbO_2-ZrO_2$  electrodes were prepared by anodic oxidation method in the lead nitrate plating bath containing  $ZrO_2$  nanoparticles. This method is simple, rapid and reproducible. In this work, the electrocatalytic performance of  $Ti/\beta-PbO_2-ZrO_2$  composite electrode in the zinc electrowinning was studied by doping  $ZrO_2$  nanoparticles. The phase composition and microstructure of electrode material were characterized by X-ray diffraction (XRD) and scanning electron microscopy (SEM), while the electrocatalytic activity for oxygen evolution was studied by linear sweep voltammetry (LSV) and electrochemical impedance spectroscopy (EIS). Cyclic voltammetry curves (CV) explain the relationship between the change of the morphology of the electrode materials and the number of active sites on the surface upon doping with  $ZrO_2$  nanoparticles.

## 2. MATERIALS AND METHODS

### 2.1 Reagents

ZrO<sub>2</sub> nanoparticles (vk-r30, purity >99.9%) were purchased in Guangdong, from the Huizhou Chemical Technology Company. All other chemicals and reagents were analytical grade and were purchased from Tianjin Fenchuan Chemical Reagent Company, China. All aqueous solutions are prepared by deionized, doubly distilled water.

### 2.2 Electrode preparation

#### 2.2.1 Electrodes preparation

The Ti plates (99.5%, 0.5 × 10 × 50 mm) were polished on 300-grit papers and stripped with deionized water; they were then soaked in a degreaser for 1 h and the pure titanium sheet was treated by etching in boiling aqueous 15% oxalic acid for 2 h. The surface of the titanium matrix was rinsed with deionized water, and after washing was placed in an ethanol solution. A stainless steel plate (0.5 × 20 × 100 mm) was used as the cathode.

#### 2.2.2 Ti/β-PbO<sub>2</sub>-ZrO<sub>2</sub> electrodes preparation

The Ti/β-PbO<sub>2</sub>-ZrO<sub>2</sub> composite electrode was prepared by direct current electrodeposition in the lead salt solution by doping ZrO<sub>2</sub> nanoparticles. This was based on the composition of the plating solution: Pb(NO<sub>3</sub>)<sub>2</sub>: 210 g·L<sup>-1</sup>, NaF: 0.5 g·L<sup>-1</sup>, Cu(NO<sub>3</sub>)<sub>2</sub>: 25 g·L<sup>-1</sup>, AEO (fatty alcohol polyoxyethylene): 0.5 g·L<sup>-1</sup>. The anode is a pretreated titanium sheet, and the cathode is a large area stainless steel sheet. On the basis of previous work, ZrO<sub>2</sub> nanoparticle contents of respectively 1# 0 g·L<sup>-1</sup>, 2# 5 g·L<sup>-1</sup>, 3# 7.5 g·L<sup>-1</sup>, 4# 10 g·L<sup>-1</sup>, and 5# 12.5 g·L<sup>-1</sup> were chosen[27]. Prior to the electroplating, the coating was applied to the coating of the mixed ZrO<sub>2</sub> nanoparticles.

### 2.3 Electrode characterization

The morphology of the Ti/β-PbO<sub>2</sub> anodes and Ti/β-PbO<sub>2</sub>-ZrO<sub>2</sub> studied by scanning electron microscopy (SEM, System Voltage 10 KV, Phenom ProX). The phase composition was characterized by X-ray diffraction (XRD, scan range 20~80°, XPertPowder) using Cu Kα radiation.

### 2.4 Electrochemical Measurement

All electrochemical measurements were performed with an electrochemical workstation (CHI600D, Shanghai Chenhua). A conventional three-electrode system was used in these experiments. The Ti/β-PbO<sub>2</sub> and Ti/β-PbO<sub>2</sub>-ZrO<sub>2</sub> (1 cm × 1 cm) were used as the working electrode, and a platinum sheet (1 cm × 1 cm) was the counter electrode. All potentials were given relative to the saturated calomel electrode (SCE). The electrochemical measurements for the electrolytic zinc solution (Zn<sup>2+</sup>: 50 g·L<sup>-1</sup>, H<sub>2</sub>SO<sub>4</sub>: 160 g·L<sup>-1</sup>) were carried out at the working temperature of the simulated industrial electrolysis temperature of 38°C. Linear sweep voltammetry curves were performed by scanning at a constant rate of 10 mV/s. The frequency interval of the EIS measurements ranged from 10<sup>5</sup> Hz to 0.01

Hz. The impedance data were converted into Nyquist data format and then fitted to appropriate simulative circuits.

### 3. RESULTS AND DISCUSSION

#### 3.1 Morphological analysis by SEM

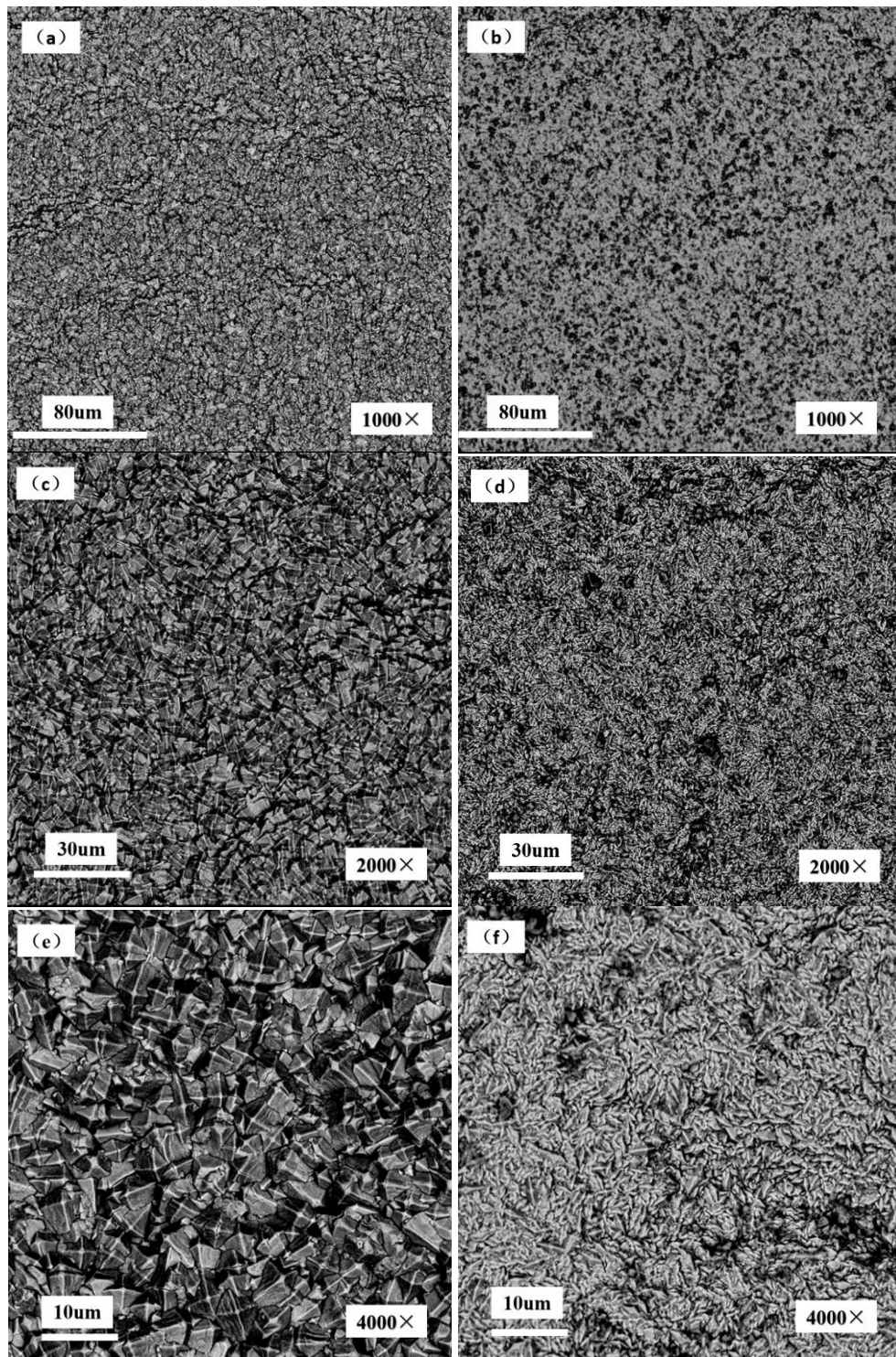


**Figure 1.** SEM images of the surfaces for (a)(c)(e) Ti/β-PbO<sub>2</sub> and (b)(d)(f) Ti/β-PbO<sub>2</sub>-ZrO<sub>2</sub>

The SEM micrographs of different electrodes are shown in Figs. 1a~f. Visually, there is a prominent difference between the electrode surface morphologies shown in Figs. 1b, 1d, and 1f. It can be seen from the above SEM images that the morphology of the two kind of electrodes is uniform and dense, presenting a typical pyramid shape. Under the same magnification, the SEM (Fig. 1e) is 4000 times larger than that of composite electrodes (Fig. 1f). The prepared composite coating has a large grain size, a relatively small specific surface area and a limited number of active sites. Fig 1f shows the sample with 10 g/L ZrO<sub>2</sub> nanoparticles at the same magnification SEM image; as is clearly seen from the diagram, in the preparation of the composite coating the grain size decreased, and the surface shows fine crystalline coating, uniform, fine crystals, fewer defects and has a larger surface area. The reason may be that ZrO<sub>2</sub> nanoparticles are deposited with lead dioxide, which increases the nucleation point and causes the crystals to become thinner. The conclusions proved that the electrode surface becomes smooth through the addition of ZrO<sub>2</sub> nanoparticles, and the grain size decreases. It is suggested that incorporation of ZrO<sub>2</sub> nanoparticles into film could improve the coating structure effectively[28].

Related research shows that the smaller grain size is favorable for the formation of large active surface area. As is well-known, a large surface area is conducive to the improvement of the catalytic performance. It is also well-known that a larger surface area is beneficial to the improvement of the oxygen evolution catalytic properties[12,29-33], so it is possible for the composite electrode doped with ZrO<sub>2</sub> to be used to improve the electrocatalytic activity in the zinc electrowinning.

### 3.2 Composition analysis by XRD

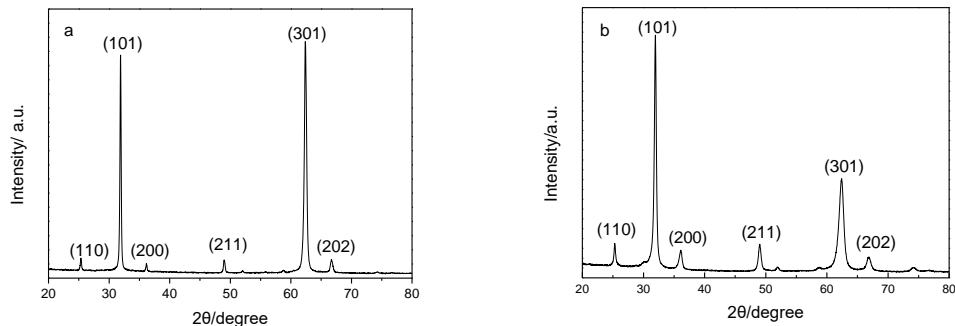


**Figure 2.** XRD patterns of (a) Ti/β-PbO<sub>2</sub> electrode and (b) Ti/β-PbO<sub>2</sub>-ZrO<sub>2</sub> electrode

The phase composition of bare Ti/β-PbO<sub>2</sub> (a) and Ti/β-PbO<sub>2</sub>-ZrO<sub>2</sub> (b) electrodes were determined by XRD, and these two kinds of electrode materials have evident characteristic diffraction peaks of the tetragonal structure of β-PbO<sub>2</sub>. It should be noted that peaks are intense at 25.4°, 31.9°, 36.3°, 49.1°, 62.5°, and 66.7° in two electrodes, and all of them are indexed to the tetragonal-shaped β-PbO<sub>2</sub> (PDF 41-1492). Obvious differences can be found through comparing two curves. The peaks at 25.4°, 31.9°, 36.3°, 49.1° and 66.7°, which belong to the Ti/β-PbO<sub>2</sub>-ZrO<sub>2</sub> electrodes (Fig. 2b), are stronger than those of the Ti/β-PbO<sub>2</sub> electrodes (Fig. 2a), and the peak at 62.5° is weaker. The bare PbO<sub>2</sub> electrode exhibits a preferred orientation along the (301) plane. Compared to the bare Ti/PbO<sub>2</sub>

electrode, the diffraction peak of Ti/ $\beta$ -PbO<sub>2</sub>-ZrO<sub>2</sub> is sharp, and the half-width of the diffraction peak is widened. It can be inferred that after doping the ZrO<sub>2</sub> nanoparticle, the PbO<sub>2</sub> electrodes were modified to make the PbO<sub>2</sub> electrode crystallize better, the grain was more refined, which shows the different preferred growth surface, the PbO<sub>2</sub> electrode is more crystalline and has a finer grain size. Thus the Ti/ $\beta$ -PbO<sub>2</sub>-ZrO<sub>2</sub> is preferred electrode material for electrolytic zinc [34,35]. This is consistent with the pattern in Fig. 1.

### 3.3 Linear sweep voltammetry analysis

The reaction of oxygen evolution (OER) occurs in the region where the current density begins to increase in the linear sweep voltammetry curve[36,37]. Therefore, the technology of LSV is an effective means to measure the oxygen evolution electrocatalytic activity of the electrode material[38]. Figure 3 shows that the effect of different additive ZrO<sub>2</sub> nanoparticles on electrochemical activity in zinc electrowinning is described by electrodeometric polarization curves. Table 1 is the corresponding oxygen response line dynamics parameter. Ti/ $\beta$ -PbO<sub>2</sub> anodes show weaker electrocatalytic activity compared to Ti/ $\beta$ -PbO<sub>2</sub>-ZrO<sub>2</sub> anodes. With the addition of ZrO<sub>2</sub> nanoparticles, the onset potential of oxygen precipitation ( $E_{onset}$ ) becomes more negative. The overpotential of oxygenation evolution reaction is significantly reduced, the oxygen evolution is easier to carry out, and the electrocatalytic performance of the electrode material is significantly improved.

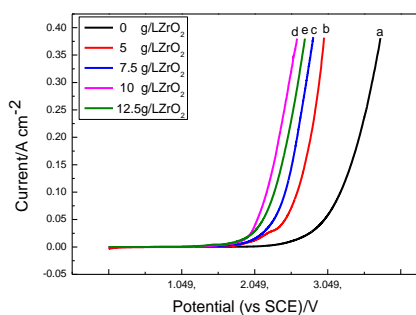


**Figure 3.** Linear sweep voltammetry curves for the addition of different ZrO<sub>2</sub>. a 1#, b 2#, c 3#, d 4#, e 5#

**Table 1.** The kinetic parameters of oxygen evolution curves of electrode prepared at different ZrO<sub>2</sub> concentrations

electrodes	a/V	b/V dec <sup>-1</sup>	j/A cm <sup>-2</sup>	E <sub>onset</sub> /V
1#	2.438	0.684	$2.727 \times 10^{-4}$	2.752
2#	1.859	0.668	$1.648 \times 10^{-3}$	2.701
3#	1.958	0.506	$1.350 \times 10^{-4}$	2.625
4#	1.530	0.434	$2.983 \times 10^{-4}$	2.465
5#	1.809	0.504	$2.575 \times 10^{-4}$	2.473

From the electrochemical catalysis point of view,  $a$  indicates the overpotential value of the current density of  $1 \text{ Acm}^{-2}$ , and  $a$ 's values are related to these factors, including the properties of the electrode material, the surface state of the electrode, the composition of the solution, the temperature solution and so on;  $b$  is a constant that is related to the temperature. In the electrolysis production, the voltage of the slot is reflected in the magnitude of  $a$ ; the smaller the  $a$  values, the lower the voltage, and the lower energy consumption. In contrast, the larger the  $a$  values, the higher the voltage. The reversibility of the electrode reaction and the susceptibility to polarization can be judged from the magnitude of the exchange current density. The greater value of the exchange current density indicates the rate of the electrode reaction is faster and the reversibility of electrode reaction is larger. Therefore, the depolarization becomes stronger. In other words, the electrode system is less susceptible to polarization, and the electrode reaction proceeds more easily. The results obtained above show that the prepared electrode material has the maximum exchange current density, and the faster electrode reaction rate when the amount of  $\text{ZrO}_2$  nanoparticles added is  $5 \text{ g/L}$  and  $10 \text{ g/L}$ . These results indicate that the electrode has a stronger electrocatalytic performance. The electrode has a lower oxygen evolution potential when the addition amount of  $\text{ZrO}_2$  is  $10 \text{ g/L}$  and  $12.5 \text{ g/L}$ , indicating that the plating process that consumes less energy and oxygen is preferentially precipitated; this conclusion is consistent with above figure 1 SEM graphs[28].

Analysis of the Tafel region is another classic method to evaluate catalytic activity of electrode materials and to further investigate whether the addition of  $\text{ZrO}_2$  nanoparticles improves the electrocatalytic activity of electrode materials[23]. In this work, the slope of the Tafel curve of an anodic material was studied. In the process of polarization, the Tafel slope is changed due to the control of oxygen evolution reaction steps, and the oxygen evolution reaction speed is caused by the area of effective activation of oxygen adsorption[31]. The smaller the  $b$  value, the smaller the overpotential, and the more favorable the reaction will be. The Tafel slope is shown in table 1, the addition of  $\text{ZrO}_2$  is  $10 \text{ g/L}$ , and the value of  $b$  is 0.43. The  $b$  value is the smallest of all samples, indicating the best catalytic performance.

### 3.4 Electrochemical impedance spectroscopy analysis

In addition, EIS studies were employed to further investigate the electrochemical properties of  $\text{ZrO}_2$  nanoparticles' doped lead dioxide anodes. Figs. 4a and b present the Nyquist plot and the equivalent circuit for these anodes, respectively. EIS simulation results were obtained by fitting the experimental data using an equivalent circuit model as displayed in Table2. The EIS data of all tested electrodes fit the equivalent circuit  $L_lR_s(C_{dl}(R_{ct})(CR_a))$  very well. In this circuit,  $L_l$  represents the solution inductance[39],  $R_s$  represents the solution resistance,  $C_{dl}$  represents the double layer,  $C_a$  and  $R_a$  are the adsorption capacity and adsorption resistance for the oxygen evolution reaction intermediates.

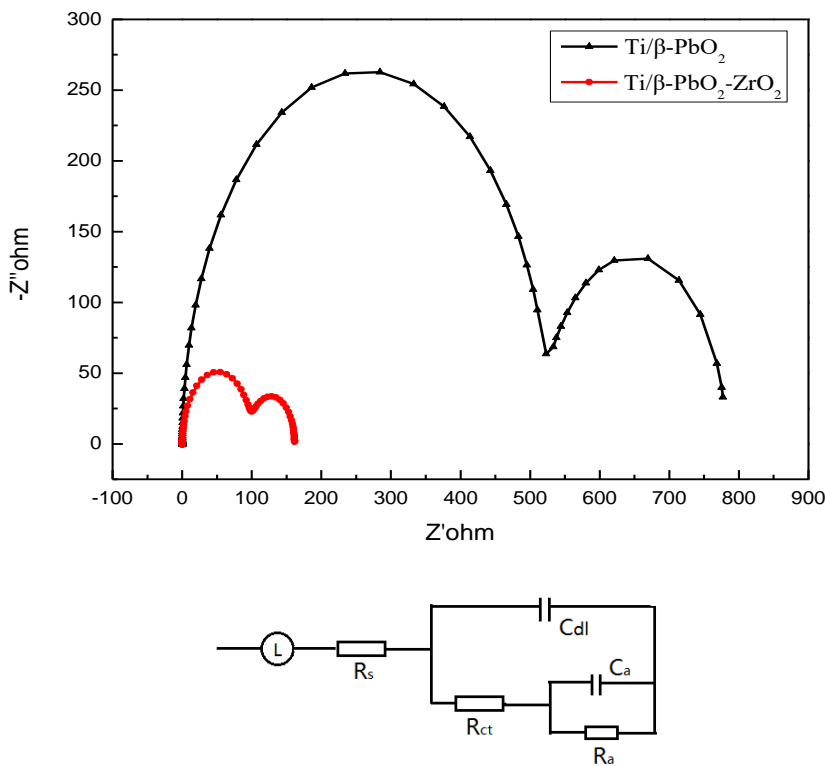


**Figure 4.** Nyquist plots of  $\text{Ti}/\beta\text{-PbO}_2$  electrode and  $\text{Ti}/\beta\text{-PbO}_2\text{-ZrO}_2$  composite electrode and equivalent circuit model in zinc electrowinning

**Table 2.** EIS simulating parameters of  $\text{Ti}/\beta\text{-PbO}_2$  electrode and  $\text{Ti}/\beta\text{-PbO}_2\text{-ZrO}_2$  composite electrode

electrodes	$L_l$ ( $10^{-6}$ )	$R_s$ ( $\Omega \text{ cm}^2$ )	$C_{dl}$ ( $\text{F cm}^{-2}$ ) ( $10^{-5}$ )	$R_{ct}$ ( $\Omega \text{ cm}^2$ )	$C$ ( $\text{F cm}^{-2}$ )	$R_a$ ( $\Omega \text{ cm}^2$ )
$\text{Ti}/\beta\text{-PbO}_2$	1.141	0.3309	2.185	527.1	0.006626	254
$\text{Ti}/\beta\text{-PbO}_2\text{-ZrO}_2$	1.168	0.2831	8.035	101.6	0.005925	59.75

The data can be seen from Table 2, the  $R_a$  value of  $\text{Ti}/\beta\text{-PbO}_2$  adsorption resistance is large, showing that the oxygen evolution reaction proceeds mainly by the formation and control of adsorbed intermediates, and the oxygen evolution reaction is the rate controlling step. The charge transfer resistance  $R_{ct}$  reflects the degree of the difficulty of the prepared electrode material in the oxygen evolution reaction[40]; in industrial electrolytic zinc electrowinning in general, the semicircle radius is smaller, and the electrochemical reaction rate is faster. Fig 5 shows the results for two doped zirconia, and it is clear the curve radius is reduced by about half. As seen from table 2, with doped  $\text{ZrO}_2$ , the  $R_{ct}$  electrode is greatly reduced, and the oxygen evolution reaction must overcome a smaller energy barrier, conducive to the effective electron transfer. The produced  $\text{ZrO}_2$  doped nanometer anode

material prepared in industrial electrolytic zinc solution is more prone to the oxygen evolution reaction. It can be seen from the table that after doping nano  $\text{ZrO}_2$ , the  $R_{ct}$  of the lead dioxide electrode is greatly reduced, which is favorable for the effective transfer of electrons. The results show that the prepared anode material is more likely to show the oxygen evolution reaction in the industrial electrolytic zinc solution.

Based on the EIS data described above combined with the SEM and XRD data, it can be inferred that grain refinement and preferred orientation changes on the surface of the  $\text{PbO}_2$  electrodes can significantly affect the  $\text{PbO}_2$  electrode material response for the charge transfer resistance and the adsorption resistance when doped with  $\text{ZrO}_2$  nanoparticles. Furthermore, the addition  $\text{ZrO}_2$  nanoparticles is mostly likely the intrinsic origin of the increase in the electrocatalytic performance of the anode material.  $\text{ZrO}_2$  is usually considered to be an inert material because  $\text{ZrO}_2$  nanoparticles are not involved in the redox processes in the deposition process, but they are not completely "inert" because they affect the deposition kinetics of nuclear sites such as  $[\text{MO}_2]\text{Pb}^{2+}_{\text{ads}}$  or  $\text{OH}_{\text{ads}}$  [41]. The addition of zirconium greatly increases the active surface area of the electrode, possibly providing more active sites for the oxygen reaction.

### 3.4 Cyclic Voltammetry analysis

The amount of the electrochemically active surface area is related to the number of active sites in the electrolytic reaction in the electrolyte. While the effective reaction area of the electrode is related to the physical specific surface area of the electrode, the physical specific surface area during the electrochemical reaction is not the same as the active sites of the electrochemical reaction. Thus, the effective reaction surface of the electrochemical reaction cannot be simply measured by the size of the physical specific surface area but rather by the electrochemically active surface area of the electrode surface.

In this work, the electrocatalytic activity of  $\text{Ti}/\beta\text{-PbO}_2$  composite doped with 10 g/L  $\text{ZrO}_2$  nanoparticles and  $\text{Ti}/\beta\text{-PbO}_2$  without doping was investigated. Fig 4 shows the cyclic voltammetry curves of two electrodes measured at the sweep speed of 0.01 V/S in the 38°C zinc electrowinning. It can be seen from Fig. 4 that the  $\text{Ti}/\beta\text{-PbO}_2$  electrode and  $\text{Ti}/\beta\text{-PbO}_2\text{-ZrO}_2$  composite electrode show the same variation in the same measurement range, and there is no obvious oxidation peak in the positive scanning process. However, with the increase of the potential, a rapid increase is observed in the anodic oxidation current, forming an oxidation branch between 2.5 V and 3.2 V. The reaction corresponding to the oxidation branch formed in this potential interval is the oxygen evolution reaction. A reduction peak is present, corresponding mainly to the transformation of  $\text{Pb}^{4+}$  to  $\text{Pb}^{2+}$  during the reverse scanning process in the 0.45~1 V range. The lack of symmetry of the oxidation branches and the peak of the reduction thus shows that the anode material in the zinc electrowinning in the redox process exhibits poor reversibility. However, it was found that the redox current density of the doped nanoparticles was significantly larger than that of the undoped  $\text{ZrO}_2$  nanoparticles when the potential was in the potential interval of the oxygen evolution. The reaction current density was higher

than that of the unconcentrated electrode current density under the same conditions. Therefore, this shows that Ti/ $\beta$ -PbO<sub>2</sub>-ZrO<sub>2</sub> composite electrode has a high electrocatalytic activity[42].

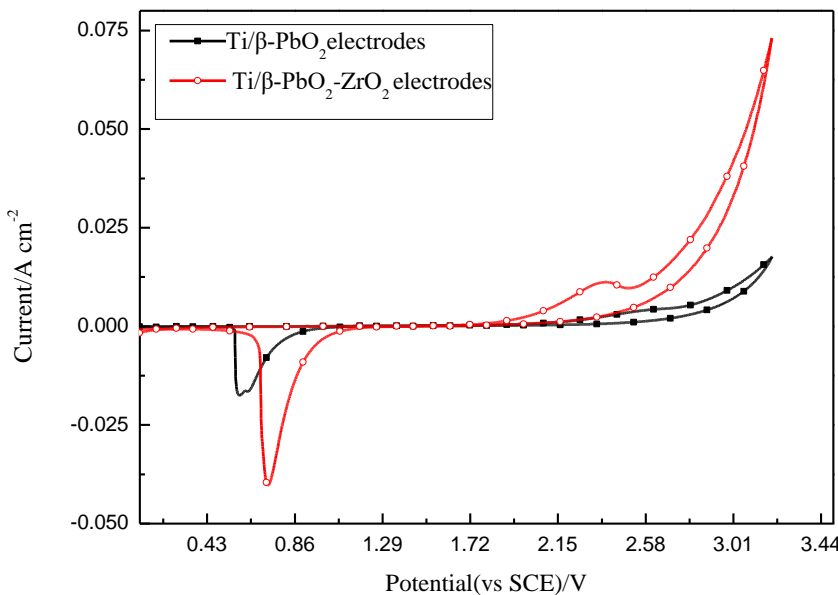
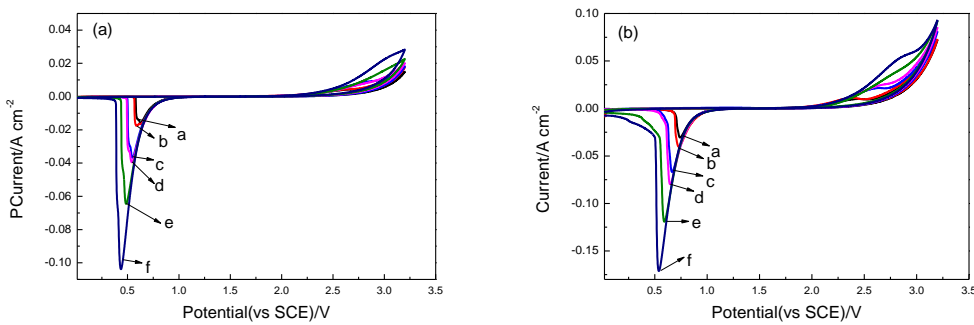


**Figure 5.** CV of Ti/β-PbO<sub>2</sub> electrode and Ti/β-PbO<sub>2</sub>-ZrO<sub>2</sub> composite electrode in zinc electrowinning (scan rate 10 mv/s)

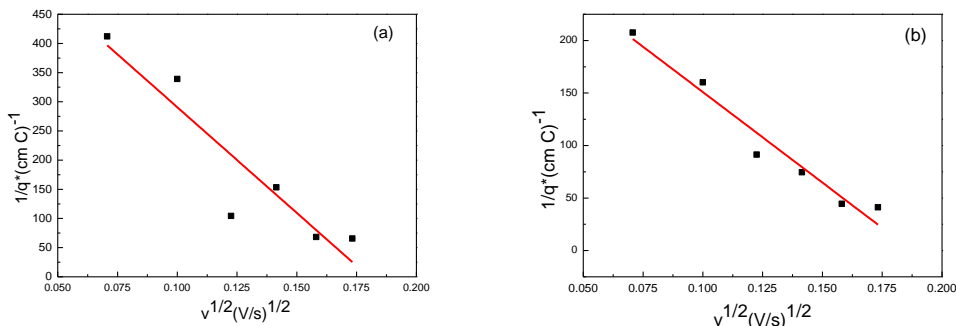
The electrocatalytic activity of the oxide coated anode material is determined by the intrinsic properties of the electrode material and the number of active sites on its surface. The intrinsic properties of the electrode material are determined by the electronic configuration of the electrode material, and the number of surface active sites of the electrode is related to the surface properties of the anode material. Electrode surface microstructure is fairly complex, and the electrode surface will form two interfaces in the electrochemical system: the first is the macroscopic interface called the outer surface between the metal oxide and electrolyte. The second interface, known as the inner surface, is the micro-interface between the metal oxide electrode and the electrolyte. The true electrochemical surface area and the magnitude of the true current density are determined by the number of active sites on both interfaces. The number of active sites affects the electrocatalytic performance of the electrode[43,44].

Fig 5 shows two different electrode material cyclic voltammetry curves in the electrolytic zinc electrowinning. It is possible to obtain the voltammetric charge that reflects the number of surface active sites of the electrode by integrating the corresponding cyclic voltammetry curve. With the increase of the scanning speed, the voltammetric charge  $q^*$  decreases as the potential changes, so the total electrochemical active surface charge is obtained at a smaller scanning speed. The voltammetric charge  $q^*$  of different electrodes can be obtained by integrating the resulting cyclic voltammetry curve to calculate the total electrochemically active surface charge of the electrode according to the following formula:  $(q^*)^{-1} = (q_T^*)^{-1} + kv^{1/2}$ [44-47]. The relationship between  $q^*$  and  $v$  is shown in Fig 6, and the number of electrochemically active surface charges of the electrode material can be obtained

by linear fitting from the obtained point in Fig 7. The results are shown in Table 3. Comparison of the Ti/ $\beta$ -PbO<sub>2</sub> electrode and Ti/ $\beta$ -PbO<sub>2</sub>-ZrO<sub>2</sub> composite electrode shows that the electrochemical active surface charge of the latter is about twice that of the former. Therefore, it can be determined that the addition of the ZrO<sub>2</sub> nanoparticles increases not only the physical specific surface area of the Ti/ $\beta$ -PbO<sub>2</sub> electrode but also the number of surface active sites of the electrode material, providing more active sites for the oxygen evolution reaction.



**Figure 6.** Cyclic voltammograms of Ti/ $\beta$ -PbO<sub>2</sub> (a) Ti/ $\beta$ -PbO<sub>2</sub>-ZrO<sub>2</sub> (b) composite electrode in zinc electrowinning at various scan rates a 0.005 V/s, b 0.01 V/s, c 0.02 V/s, d 0.03 V/s, e 0.04 V/s, f 0.045 V/s



**Figure 7.** Relationship between  $q^*$  and  $v$  of the Ti/ $\beta$ -PbO<sub>2</sub> (a) and Ti/ $\beta$ -PbO<sub>2</sub>-ZrO<sub>2</sub> composite electrode(b)

**Table 3.**  $q_T^*$  of PbO<sub>2</sub> electrode and PbO<sub>2</sub>-ZrO<sub>2</sub> composite electrode

Electrode	$q_T^*$ (C/cm <sup>2</sup> )
Ti/ $\beta$ -PbO <sub>2</sub> electrodes	0.015
Ti/ $\beta$ -PbO <sub>2</sub> -ZrO <sub>2</sub> composite electrodes	0.031

#### 4. CONCLUSIONS

1. By analyzing the anode polarization curve in the Ti/ $\beta$ -PbO<sub>2</sub>-ZrO<sub>2</sub> composite electrode, it is found that the optimal addition to PbO<sub>2</sub> is 10 g/L ZrO<sub>2</sub> nanoparticles, obtaining a composite anode

material that has a larger current density than the pure  $\text{PbO}_2$  electrodes and reducing the oxygen potential by 0.28 V. Therefore, the best amount of added  $\text{ZrO}_2$  nanoparticles for the  $\text{Ti}/\beta\text{-PbO}_2\text{-ZrO}_2$  composite electrode is 10 g/L.

2. Through the analysis of the Nyquist diagram and related data, the  $\text{Ti}/\text{PbO}_2\text{-ZrO}_2$  electrode prepared with the doping of 10 g/L shows a smaller capacitive reactance arc, explaining why the oxygen evolution reaction in electrolytic zinc liquid needs to overcome a smaller base and showing a faster electrode reaction rate and high electric catalytic activity.

3. Through the analysis of cyclic voltammetry, electrochemical active surface charge of the anode material prepared by adding 10 g/L  $\text{ZrO}_2$  nanoparticles is found to be two times larger than that for the electrode material without adding  $\text{ZrO}_2$ ; SEM and XRD and a combination of the two kinds of electrode material microstructure and phase composition analysis techniques show that the addition of  $\text{ZrO}_2$  electrode material increases not only the physical surface area but also the charge number of the electrochemically active surface, providing more active sites for the oxygen evolution reaction and resulting in good electrocatalytic activity.

#### ACKNOWLEDGEMENTS

This work was financially supported by the Natural Science Foundation of China (51464021)

#### References

1. C.j. Yang, S.-M. Park, *Electrochim. Acta*, 108 (2013) 86.
2. A. Guerfi, J. Trottier, I. Boyano, I. De Meatza, J.A. Blazquez, S. Brewer, K.S. Ryder, A. Vijh, K. Zaghib, *J. Power Sources*, 248 (2014) 1099.
3. I. Ivanov, Y. Stefanov, Z. Noncheva, M. Petrova, T. Dobrev, L. Mirkova, R. Vermeersch, J.P. Demaerel, *Hydrometallurgy*, 57 (2000) 125.
4. I. Ivanov, Y. Stefanov, Z. Noncheva, M. Petrova, T. Dobrev, L. Mirkova, R. Vermeersch, J.P. Demaerel, *Hydrometallurgy*, 57 (2000) 109.
5. R.H. Newnham, *J. Appl. Electrochem.*, 22 (1992) 116.
6. W. Zhang, E. Ghali, G. Houlachi, *Mater. Technol.*, 29 (2014) A48.
7. D. Kong, *Prog. Chem.*, 21 (2009) 1107.
8. G. Darabizad, M.S. Rahmanifar, M.F. Mousavi, A. Pendashteh, *Mater. Chem. Phys.*, 156 (2015) 121.
9. R.G. Saratale, K.J. Hwang, J.Y. Song, G.D. Saratale, D.S. Kim, *J. Environ. Eng.*, 142 (2016) 04015064.
10. X. Li, D. Pletcher, F.C. Walsh, *Chem. Soc. Rev.*, 40 (2011) 3879.
11. M. Mohammadi, F. Mohammadi, G. Houlachi, A. Alfantazi, *J. Electrochem. Soc.*, 160 (2013) E27.
12. D. Devilliers, E. Mahé, *Electrochim. Acta*, 55 (2010) 8207.
13. I. Sirés, C.T.J. Low, C. Ponce-de-León, F.C. Walsh, *Electrochim. Acta*, 55 (2010) 2163.
14. A.B. Velichenko, R. Amadelli, V.A. Knysh, T.V. Luk'yanenko, F.I. Danilov, *J. Electroanal. Chem.*, 632 (2009) 192.
15. F.L. Souza, J.M. Aquino, K. Irikura, D.W. Miwa, M.A. Rodrigo, A.J. Motheo, *Chemosphere*, 109 (2014) 187.
16. H.Y. Zhao, J.L. Cao, F.H. Cao, J.Q. Zhang, *Chinese J. Inorg. Chem.*, 25 (2009) 117.
17. X.L. Liu, Y.Y. Dan, L.U. Hai-Yan, H.B. Lin, M.L. Ouyang, C.J. Yun, *J. Electrochem.*, 19 (2013) 59.
18. S. Cattarin, M. Musiani, *Electrochim. Acta*, 52 (2007) 2796.

19. S. Ghasemi, M.F. Mousavi, H. Karami, M. Shamsipur, S.H. Kazemi, *Electrochim. Acta*, 52 (2006) 1596.
20. H.S. Kong, W.M. Huang, H.B. Lin, H.Y. Lu, W.L. Zhang, *Chin. J. Chem.*, 30 (2012) 2059.
21. Y. Dan, H. Lu, X. Liu, H. Lin, J. Zhao, *Int. J. Hydrogen Energ.*, 36 (2011) 1949.
22. Y. Yao, L. Jiao, L. Cui, N. Yu, F. Wei, Z. Lu, *J. Electrochem. Soc.*, 162 (2015) H693.
23. M. Musiani, F. Furlanetto, R. Bertoncello, *J. Electroanal. Chem.*, 465 (1999) 160.
24. Y. Yao, H. Dong, L. Jiao, N. Yu, L. He, *J. Electrochem. Soc.*, 163 (2016) D179.
25. Y.Qiang C.Zhen, F.YingYing, *J.Mater.Eng.*, (2014) 40.
26. M. Xu, Z. Wang, F. Wang, P. Hong, C. Wang, X. Ouyang, C. Zhu, Y. Wei, Y. Hun, W. Fang, *Electrochim. Acta*, 201 (2016) 240.
27. Y. Yao, M. Zhao, C. Zhao, H. Zhang, *Electrochim. Acta*, 117 (2014) 453.
28. OliveiraSousa, A. Delimaneto, P. De, *J. Braz. Chem. Soc.*, 13 (2002) 218.
29. M.A. Ajeel, M.K. Aroua, W.M.A.W. Daud, S.A. Mazari, *Ind. Eng. Chem. Res.*, 56 (2017) 1652.
30. S. Tong, T. Zhang, C.a. Ma, *Chin. J. Chem. Eng.*, 16 (2008) 885.
31. Y.F. He, J.T. Feng, Y.Y. Du, D.Q. Li, *Acs Catal.*, 2 (2012) 1703.
32. Y. Zhao, J. Zhang, *J. Appl. Crystallogr.*, 41 (2008) 1095.
33. X. Li, X. Li, W. Yang, X. Chen, W. Li, B. Luo, K. Wang, *Electrochim. Acta*, 146 (2014) 15.
34. H. Li, Y. Chen, Y. Zhang, W. Han, X. Sun, J. Li, L. Wang, *J. Electroanal. Chem.*, 689 (2013) 193.
35. M. Panizza, G. Cerisola, *Cheminform*, 41 (2010) 6570.
36. E. Tsuji, A. Imanishi, K.I. Fukui, Y. Nakato, *Electrochim. Acta*, 56 (2011) 2009.
37. X.L. Li, H. Xu, W. Yan, *Appl. Surf. Sci.*, 389 (2016) 278.
38. X. Duan, C. Zhao, W. Liu, X. Zhao, L. Chang, *Electrochim. Acta*, 240 (2017) 424.
39. R. Amadelli, L. Samiolo, A.B. Velichenko, V.A. Knysh, T.V. Luk'yanenko, F.I. Danilov, *Electrochim. Acta*, 54 (2009) 5239.
40. Y. He, W. Huang, R. Chen, W. Zhang, H. Lin, H. Li, *Sep. Purif. Technol.*, 156 (2015) 124.
41. S. Trasatti, *Electrochim. Acta*, 36 (1991) 225.
42. C. Comninellis, G.P. Vercesi, *J Appl. Electrochem.*, 21 (1991) 335.
43. H. Vogt, *Electrochim. Acta*, 39 (1994) 1981.
44. K.W. Kim, E.H. Lee, J.S. Kim, K.H. Shin, K.H. Kim, *Electrochim. Acta*, 46 (2002) 915.
45. S. Liu, Y. Wang, X. Zhou, W. Han, J. Li, X. Sun, J. Shen, L. Wang, *Electrochim. Acta*, 253 (2017) 357.